AFRL-ML-WP-TP-2006-402

AN EXPERIMENTAL INVESTIGATION OF GUIDED WAVE PROPAGATION IN CORRUGATED PLATES SHOWING STOP BANDS AND PASS BANDS (PREPRINT)

T. Kundu, S. Banerjee, and Kumar V. Jata

FEBRUARY 2006

Approved for public release; distribution is unlimited.

STINFO FINAL REPORT

MATERIALS AND MANUFACTURING DIRECTORATE
AIR FORCE RESEARCH LABORATORY
AIR FORCE MATERIEL COMMAND
WRIGHT-PATTERSON AIR FORCE BASE, OH 45433-7750

NOTICE

Using Government drawings, specifications, or other data included in this document for any purpose other than Government procurement does not in any way obligate the U.S. Government. The fact that the Government formulated or supplied the drawings, specifications, or other data does not license the holder or any other person or corporation; or convey any rights or permission to manufacture, use, or sell any patented invention that may relate to them.

This report was cleared for public release by the Air Force Research Laboratory Wright Site (AFRL/WS) Public Affairs Office (PAO) and is releasable to the National Technical Information Service (NTIS). It will be available to the general public, including foreign nationals.

PAO Case Number: AFRL/WS 06-0555, 27 Feb 06.

THIS TECHNICAL REPORT IS APPROVED FOR PUBLICATION.

/s/

KUMAR V. JATA

/s/

GERALD J. PETRAK, Asst Chief
Metals, Ceramics and NDE Division
Materials and Manufacturing Directorate

/s/

GERALD J. PETRAK, Asst Chief
Metals, Ceramics and NDE Division
Materials and Manufacturing Directorate

This report is published in the interest of scientific and technical information exchange and its publication does not constitute the Government's approval or disapproval of its ideas or findings.

REPORT DOCUMENTATION PAGE

Form Approved
OMB No. 0704-0188

1. REPORT DATE *(DD-MM-YY)*	2. REPORT TYPE	3. DATES COVERED *(From - To)*
February 2006	Journal Article Preprint	

4. TITLE AND SUBTITLE

AN EXPERIMENTAL INVESTIGATION OF GUIDED WAVE PROPAGATION IN CORRUGATED PLATES SHOWING STOP BANDS AND PASS BANDS (PREPRINT)

5a. CONTRACT NUMBER
FA8650-04-C-5228

5b. GRANT NUMBER

5c. PROGRAM ELEMENT NUMBER
63112F

6. AUTHOR(S)

T. Kundu and S. Banerjee (University of Arizona)
Kumar V. Jata (AFRL/MLLP)

5d. PROJECT NUMBER
3153

5e. TASK NUMBER
40

5f. WORK UNIT NUMBER
41300100

7. PERFORMING ORGANIZATION NAME(S) AND ADDRESS(ES)

University of Arizona
Department of Civil Engineering
and Engineering Mechanics
Tucson, AZ 85721

Nondestructive Evaluation Branch (AFRL/MLLP)
Metals, Ceramics and NDE Division
Materials and Manufacturing Directorate
Air Force Research Laboratory, Air Force Materiel Command
Wright-Patterson AFB, OH 45433-7750

8. PERFORMING ORGANIZATION REPORT NUMBER

9. SPONSORING/MONITORING AGENCY NAME(S) AND ADDRESS(ES)

Materials and Manufacturing Directorate
Air Force Research Laboratory
Air Force Materiel Command
Wright-Patterson AFB, OH 45433-7750

10. SPONSORING/MONITORING AGENCY ACRONYM(S)
AFRL/MLLP

11. SPONSORING/MONITORING AGENCY REPORT NUMBER(S)
AFRL-ML-WP-TP-2006-402

12. DISTRIBUTION/AVAILABILITY STATEMENT

Approved for public release; distribution is unlimited.

13. SUPPLEMENTARY NOTES

Report contains color.

14. ABSTRACT

For health monitoring of structures with periodic geometry a good understanding of the elastic wave propagation through such periodic structures is necessary. Although a number of research papers on the wave propagation through periodic structures are available in the literature hardly anyone investigated experimentally the guided wave propagation through plates with periodic plate boundaries and compared the experimental data with theoretical predictions. In this paper the elastic wave propagation in three different plates with different degrees of corrugation is experimentally studied. The experimental results clearly show that elastic waves can propagate through the corrugated plate (waveguide) for certain frequencies called pass bands and find it difficult to propagate for some other frequencies called stop bands. Stop bands are found to increase with the degree of corrugation. Experimental results for non-sinusoidal periodic plates are compared with the theoretical predictions for sinusoidal corrugated plates and good matching is observed for plates with small degree of corrugation indicating that for small corrugation depths only two parameters – the depth of corrugation and the wavelength of the periodicity – are enough for modeling the elastic wave propagation through the corrugated plate.

15. SUBJECT TERMS

Structural health monitoring, guided waves

16. SECURITY CLASSIFICATION OF:			17. LIMITATION OF ABSTRACT:	18. NUMBER OF PAGES	19a. NAME OF RESPONSIBLE PERSON (Monitor)
a. REPORT	b. ABSTRACT	c. THIS PAGE			Kumar V. Jata
Unclassified	Unclassified	Unclassified	SAR	32	19b. TELEPHONE NUMBER *(Include Area Code)*

Standard Form 298 (Rev. 8-98)
Prescribed by ANSI Std. Z39-18

This work has been submitted for publication in the Journal of the Acoustical Society of America

An Experimental Investigation of Guided Wave Propagation in Corrugated Plates showing Stop Bands and Pass Bands

T. Kundu[1], S. Banerjee[2] & K. V. Jata[3]

[1, 2]Department of Civil Engineering and Engineering Mechanics, University of Arizona, Tucson, Arizona 85721
[3]Air Force Research Laboratory, AFRL/MLL
Wright Patterson Air Force Base Ohio 45433

Email: tkundu@email.arizona.edu[1], souravban@netscape.net[2],Kumar.Jata@wpafb.af.mil[3]

ABSTRACT

Non-planar surfaces are often encountered in engineering structures. Periodically corrugated boundaries can be found in aerospace structural components such as the surface formed by friction stir welding, and in civil structural components such as rebars used inside reinforced concrete beams and slabs. Engineers and architects are also designing periodic structures to create desired acoustic band gaps. For health monitoring of structures with periodic geometry a good understanding of the elastic wave propagation through such periodic structures is necessary. Although a number of research papers on the wave propagation through periodic structures are available in the literature hardly anyone investigated experimentally the guided wave propagation through plates with periodic plate boundaries and compared the experimental data with theoretical predictions. In this paper the elastic wave propagation in three different plates with different degrees of corrugation is experimentally studied. The experimental results clearly show that elastic waves can propagate through the corrugated plate (waveguide) for certain frequencies called pass bands and find it difficult to propagate for some other frequencies called stop bands. Stop bands are found to increase with the degree of corrugation. Experimental results for non-sinusoidal periodic plates are compared with the theoretical predictions for sinusoidal corrugated plates and good matching is observed for plates with small degree of corrugation indicating that for small corrugation depths only two parameters – the depth of corrugation and the wavelength of the periodicity – are enough for modeling the elastic wave propagation through the corrugated plate.

KEY WORDS: Guided wave, Stop band, Pass band, Waveguide, Corrugated plate, Non-planar structure.

Running Title: Wave propagation in corrugated plates

PREPRINT

Introduction

The problem of elastic wave propagation in periodic structures has been investigated for over five decades. Brillouin wrote the classical book on this subject in 1946. Dynamics of a wide variety of periodic structures has been presented in this book. Later Mead and his co-workers (Mead, 1970, 1975, 1976, 1986; Mead and Markus, 1983; Mead and Bardell, 1987; Mead and Yaman, 1991) made significant contributions in this field of research. In these works Mead et. al. solved the elasto-dynamic problems involving periodically supported beams (Mead, 1970; Mead and Markus, 1983), periodic damped plates (Mead, 1976), damped plates with stiffeners (Mead, 1986; Mead and Yaman, 1991) and thin cylindrical shells with periodic circumferential stiffeners (Mead and Bardell, 1987). Like many other engineering problems the dynamics of periodic structure has been also solved by the finite element method (Oris and Petyt, 1974). Following Brillouin's classical approach recently Ruzzene and Baz (2000) analytically solved the one-dimensional problem of elastic wave propagation in composite rods with shape memory alloy inserts, periodically embedded in the base material of the rod. Interested readers are referred to the article by Mester and Benaroya (1995) for a comprehensive review of wave propagation problems in periodic and near-periodic structures.

A common feature of the elastic wave propagation in periodic structures is the existence of distinct frequency bands – some of which allow wave propagation and others do not. Those frequencies, for which the waves can propagate through the structure, are called pass band frequencies and other frequencies for which the waves are attenuated in the structure are called stop band frequencies. The stop bands are also sometimes called forbidden frequency bands (Vasseur et. al., 1998).

In none of the articles referred above the elastic wave propagation through free plates with periodic surface boundaries has been analyzed. In the above papers the periodicity inside the materials or in the support condition has been considered. For example Brillouin (1946) in his classical book presented the solution of wave propagation problem through one, two and three-dimensional lattices of point masses with various degrees of complexity, Vasseur et. al. (1998) studied the wave transmission through two-dimensional binary solid/solid composite media composed of arrays of Duralumin cylindrical inclusions embedded in an epoxy resin matrix, Ruzzene and Baz (2000) solved the one-dimensional wave propagation problem through a composite rod with periodical insertions.

The problem of wave propagation in structures made of homogeneous materials but having non-planar boundaries and interfaces has been the topic of investigation in last three decades (Nayfeh et al, 1978; Boström, 1983, 1989; Standström, 1986; Fokkemma, 1980; Glass et al. 1983; El-Bahrawy, 1994a, 1994b; Banerjee and Kundu, 2004; Declercq et al, 2005). Stop bands and pass bands of the Rayleigh-Lamb symmetric modes in sinusoidally corrugated waveguides have been studied by El-Bahrawy (1994a). Only recently generalized dispersion equations for periodically corrugated waveguides have been studied and solutions for both symmetric and anti-symmetric modes in a sinusoidally corrugated waveguide have been presented (Banerjee and Kundu, 2006).

Although a number of theoretical papers have been published on elastic wave propagation in periodic structures, as mentioned above, very few experimental papers are available on this topic. Vasseur et. al. (1998) experimentally obtained stop bands and pass bands in two-dimensional binary solid/solid composite media composed of arrays of Duralumin cylindrical inclusions embedded in an epoxy resin matrix. To the best of our knowledge no investigator has yet experimentally measured stop band and pass band frequencies in corrugated plates and compared the experimental results with the theoretical predictions as done in this paper.

Experiment

Transducer Characterization:

Two 0.5 inch diameter ultrasonic transducers were placed face to face as shown in Fig. 1a. One transducer was excited by a signal frequency that continuously varied from 300 kHz to 800 kHz, while the second transducer recorded the received signal. The recorded signal is shown in Fig. 1b. Note that the transducer resonance frequency is close to 540 kHz although the transducers were labeled as having 500 kHz resonance frequency.

Specimens:

Three aluminum plates were machined to produce three specimens with three different degrees of corrugation. A typical specimen is shown in Fig. 2. Figure 2a shows the full plate, Fig. 2b shows the side view of the corrugation and Fig. 2c shows the period of corrugation D, highest plate thickness H_1 and lowest plate thickness H_2 in the corrugated region. Note that the average plate thickness (2h) in the corrugated region is equal to $(H_1+H_2)/2$, and the corrugation depth $\varepsilon = (H_1-H_2)/4$. These dimensions for the 3 specimens are given in Table 1.

Table 1: Dimensions of 3 corrugated plate specimens.
All dimensions are given in inch and mm; mm values are given in parentheses.

Specimen #	H_1 $(2h+2\varepsilon)$	H_2 $(2h-2\varepsilon)$	D	2h $(H_1+H_2)/2$	ε $(H_1-H_2)/4$	2h/D	ε/D
1	0.5 (12.7)	0.416 (10.57)	0.425 (10.8)	0.458 (11.63)	0.021 (0.53)	1.078	0.049
2	0.5 (12.7)	0.3 (7.62)	0.37 (9.40)	0.4 (10.16)	0.05 (1.27)	1.081	0.135
3	0.5 (12.7)	0.187 (4.75)	0.38 (9.65)	0.344 (8.74)	0.078 (1.98)	0.905	0.205

Experimental Setup:

Two transducers are placed in the pitch-catch arrangement over the aluminum plate as shown in Fig. 3. Transducer T acts as the transmitter and the second transducer R acts as the receiver. Two transducers are inclined at an angle θ (clockwise and counter-clockwise) with respect to the vertical axis as shown. The transducers are placed at a face to face distance of 'd' and a height 'h' above the aluminum plate. Transducers and the plate are immersed in water that acts as the coupling fluid between the transducers and the plate so that the ultrasonic energy can easily propagate from the transmitter to the plate and from the plate to the receiver. If the distance d is set such that the direct reflected beam (shown by dashed line in Fig. 3) cannot reach the receiver then the ultrasonic energy must propagate through the plate for a length g_1 as the guided wave (shown by the bold arrow in Fig. 3) before leaking back into the coupling fluid and reaching the receiver R.

Experimental Results:

Experiments are carried out for two different angles of incidence, $\theta = 25^o$ and 30^o. Experimental results for these two sets of incident angles are described in detail below.

Experimental Results for 25^o *and* 30^o *angles of incidence*

Two transducers T and R of 1 inch (25.4 mm) diameter are placed above the smooth portion of the aluminum plate which is 0.5 inch (12.7 mm) thick. First, the transducers are positioned such that the directly reflected beam (shown by dashed line in Fig. 3) can reach the receiver R. This is the case when h = 3 inch (76.2 mm) and d = 2.8 inch (71.1 mm). The received signal strength as a function of the frequency for this transducer-receiver arrangement is shown in Fig. 4. Note that Figs. 1b and 4 are almost identical. Therefore, the receiving signal characteristics are not altered significantly when the transmitter and receiver are placed in the pitch-catch arrangement with the receiver receiving the direct reflected beam. The received signal is plotted after attenuating the signal by a 37 dB attenuator. When h is reduced to 2.5 inch (63.5 mm) and d is proportionately reduced to 2.3 inch (58.4 mm) then the reflected beam showed similar strength variation with frequency.

Keeping h fixed at 2.5 inch (63.5 mm) when the transducer spacing is increased to 4.25 inch (108 mm) then the received signal voltage versus frequency plot is changed significantly as shown in Fig. 5. We will call these received signal voltage versus frequency plots as V(f) curves. The V(f) curve of Fig. 5 is plotted after attenuating the received signal by a 28 dB attenuator. Note that the peak near 540 kHz observed in Figs. 1b and 4 is no longer present in Fig. 5. Also, two peaks of Fig. 5 near 430 kHz and 645 kHz are absent in Figs. 1 and 4. It will be shown later that these two peaks correspond to two Lamb wave modes in the plate. A simple calculation with transducer diameter D = 1 inch (25.4 mm), transducer spacing d = 4.25 inch (108 mm), height h = 2.5 inch (63.5 mm) and transducer inclination angle $\theta = 25^o$ gives g (see Fig. 3) = 1.918 inch (48.72 mm) and g_1 (see Fig. 3) = 0.815 inch (20.7 mm). Since g_1 is non-zero the direct reflected

beam cannot reach the receiver. Therefore, the ultrasonic energy must propagate through the plate as guided waves for certain distance greater than g_1 before leaking into the coupling fluid and being received by the receiver. It will be shown later that two frequencies 430 kHz and 645 kHz generate two guided wave modes for transducer inclination angle $\theta = 25^o$.

When the smooth plate is replaced by an aluminum plate with small corrugation (ε/D = 0.049, Specimen 1 in Table 1), the V(f) curve obtained for the setting h = 3 inch (76.2 mm) and d = 7 inch (177.8 mm) is shown in Fig. 6a. For the transducer spacing d = 7 inch, the distance traveled by the guided wave in the corrugated plate is significantly greater than that for Fig. 5. Naturally, the received signal in Fig. 6a is much weaker than that in Fig. 5. Only an attenuation of strength 16 dB is applied to the received signal before plotting it in Fig. 6a while for Fig. 5 it was 28 dB.

A comparison between Figs. 6a and 4 shows some similarities between these two V(f) curves - both have peaks between 500 and 550 kHz and the signal strength gradually decays to very small value at low (~300 kHz) and high (~800 kHz) frequencies. However, a closer inspection also reveals some clear distinctions that will be discussed later.

Keeping all parameters (h, d, θ) unchanged Specimen 1 is then replaced by Specimen 2 and finally by Specimen 3. The V(f) curve for Specimen 2 (medium corrugation, ε/D = 0.135) is shown in Fig. 6b, and for Specimen 3 (large corrugation, ε/D = 0.205) it is shown in Fig. 6c. To maintain the numerical value of the V(f) peaks close to 0.3 in all plots, a 14dB attenuator is used for Fig. 6b and 18dB attenuator is used for Fig. 6c. Comparison of these two figures with Fig. 4 shows some distinctive features that are discussed later.

Similar experiments with the same 3 corrugated plate specimens are carried out again for 30^o angle of incidence and V(f) curves for the 3 plates are recorded. Three V(f) curves for the three corrugated plates for 30^o angle of incidence are shown in Figs. 7a, b and c.

Distinctive Features of V(f) curves of Corrugated Plates

A comparison of Figs. 4 and 7a reveals that in Fig. 4 the signal strength is the maximum near 540 kHz and it decays almost monotonically for both higher and lower frequencies while that is not the case in Fig. 7a. Although the V(f) amplitude envelope has a decaying trend for both higher and lower frequencies this trend is not as monotonic as in Fig. 4. Clearly in Fig. 7a the amplitude envelope has two noticeable dips near 380 and 480 kHz, as shown by dashed curved line in Fig. 7a. A few other smaller dips may be noticed in the amplitude envelope but the two strongest dips are near 380 and 480 kHz. Note that the propagating signal amplitude is very small in the frequency ranges 370-390 kHz and 470-490 kHz. Clearly the ultrasonic signal finds it difficult to propagate in these two frequency ranges. The frequency bandwidths that block the ultrasonic wave propagation through the plate are called ‘Stop bands’ and the frequency bandwidths that do not cause such obstruction to the wave propagation are called ‘Pass bands’.

Therefore, for Specimen 1, for 30^o angle of incidence stop bands are 370-390 kHz and 470-490 kHz while the frequency bandwidths 300-370 kHz, 390-470 kHz and 490-650 kHz constitute the pass bands. Near the bottom of Fig. 7a continuous and dashed horizontal lines are used to mark pass band and stop band regions, respectively. Similarly, in Figs. 7b, 7c, 6a, 6b and 6c pass bands and stop bands are marked by continuous and dashed lines, respectively. In some figures clear distinctions exist between the signals in pass band and stop band regions. For example, in Fig. 6c signals in the pass band zones are significantly stronger than those in the stop band zones. However, in some other figures like in Fig. 7a the signal strength variations in these two regions are not that distinct. In these situations sophisticated signal processing techniques can be applied to the V(f) data to improve the stop band and pass band identification.

Stop band and pass band frequencies for the 3 plates, obtained for 30^o and 25^o angles of incidence are shown by continuous and dashed lines in Figs. 6 and 7 and their values are listed in Table 2.

Table 2: Stop band and pass band frequencies in kHz for 2 striking angles and 3 corrugated plate specimens whose dimensions are given in Table 1

Striking Angle	Spec. #1 Stop band	Spec. #1 Pass band	Spec. #2 Stop band	Spec. #2 Pass band	Spec. #3 Stop band	Spec. #3 Pass band
30^o	370-390 470-490	300-370 390-470 490-650	300-380 620-645	380-620 645-680	300-450 580-600	450-580
25^o	300-350 375-410 465-510 580-610	350-375 410-465 510-580	440-460 600-640	340-440 460-580	300-390 470-530 590-650	390-470 530-590

Dispersion Curves for Smooth Plates:

Before analyzing and understanding the experimental data for the corrugated plates given figures 6 and 7 and summarized in Table 2, it is necessary to investigate first if the V(f) curve for the smooth plate (Fig. 5) is reliable; in other words, whether the peaks of the V(f) curve for the smooth plate for which the guided wave propagation theory is well developed are appearing at the right places. Figure 5 shows its two peaks near 430 kHz and 645 kHz; these peaks are not present in Fig. 4. Do these peaks correspond to the Lamb wave modes generated in the plate? To investigate it, the dispersion curves for the aluminum plate are theoretically computed. The P-wave speed (c_P) in aluminum is 6.2 km/s, its S-wave speed (c_S) is 3 km/s, and density (ρ) is 2.7 gm/cc. The plate thickness is 12.7 mm.

Lamb wave dispersion curves for a homogeneous, isotropic, elastic plate are obtained from the well-known dispersion equations [Kundu, 2004],

$$\frac{\tanh\left(\omega h\sqrt{\frac{1}{c_L^2}-\frac{1}{c_P^2}}\right)}{\tanh\left(\omega h\sqrt{\frac{1}{c_L^2}-\frac{1}{c_S^2}}\right)}=\frac{\left(\frac{2}{c_L^2}-\frac{1}{c_S^2}\right)^2}{\frac{4}{c_L^2}\sqrt{\frac{1}{c_L^2}-\frac{1}{c_P^2}}\sqrt{\frac{1}{c_L^2}-\frac{1}{c_S^2}}} \tag{1a}$$

$$\frac{\tanh\left(\omega h\sqrt{\frac{1}{c_L^2}-\frac{1}{c_P^2}}\right)}{\tanh\left(\omega h\sqrt{\frac{1}{c_L^2}-\frac{1}{c_S^2}}\right)}=\frac{\frac{4}{c_L^2}\sqrt{\frac{1}{c_L^2}-\frac{1}{c_P^2}}\sqrt{\frac{1}{c_L^2}-\frac{1}{c_S^2}}}{\left(\frac{2}{c_L^2}-\frac{1}{c_S^2}\right)^2} \tag{1b}$$

Where ω is the angular frequency ($\omega = 2\pi f$) of the propagating wave; the signal frequency f is in MHz and ω is in rad/μsec. h is half of the plate thickness in mm, c_P and c_S are P-wave speed and S-wave speed in the plate material, respectively, and c_L is the phase velocity of the propagating Lamb wave modes. All velocities are in km/s. Equations (1a) and (1b) correspond to the symmetric and anti-symmetric Lamb modes, respectively. Dispersion curves generated by Eqn. 1 are shown in Fig. 8.

The incident angle for the V(f) curves of Fig. 5 is 25^o. Therefore, the corresponding phase velocity from Snell's law is

$$c_L = \frac{c_f}{\sin\theta} = \frac{1.49}{\sin(25)} = 3.526 \text{ km/s} \tag{2}$$

Where c_f is the acoustic wave speed in water (= 1.49 km/s) and θ is the incident angle (= 25^o). Therefore, two peaks of Fig. 5 correspond to two points in the frequency-phase velocity plot of Fig. 8. The horizontal and vertical coordinates of these points are (430 kHz, 3.526 km/s) and (645 kHz, 3.526 km/s). These points are plotted on Fig. 8 by solid circles. Note that they coincide with the A_1 (first anti-symmetric) and S_1 (first symmetric) modes. Thus the reliability of the experimental V(f) plots is established.

Dispersion Curves for Corrugated Plates:

Banerjee and Kundu (2005) presented a theoretical solution of elastic wave propagation in sinusoidal corrugated plates as shown in Fig. 9. The dispersion equation for such plates with periodic boundary geometry can be written as

$$Det\,[\mathbf{T}] = 0 \tag{3}$$

The dimension of the matrix **T** is (2*mod*(*n*)+1)x(2*mod*(*n*)+1), where *n* is the number of wave numbers developed for each frequency in the sinusoidally corrugated plate. If *n* varies from -1 to +1, the elements of the **T** matrix can be written as (Banerjee and Kundu (2005))

$$BC1_{np}^{+} = -2\mu(k_n\eta_n)\left[De^{ih\eta_n}\left(J_0(\varepsilon\eta_n)+iH_0(\varepsilon\eta_n)\right)\right]$$
$$BC1_{np}^{-} = -2\mu(-k_n\eta_n)\left[De^{-ih\eta_n}\left(J_0(\varepsilon\eta_n)-iH_0(\varepsilon\eta_n)\right)\right]$$

$$
\begin{aligned}
BC1^{+}_{ns} &= \mu(k_n{}^2 - \beta_n{}^2)\left[De^{ih\beta_n}\left(J_0(\varepsilon\beta_n) + iH_0(\varepsilon\beta_n)\right)\right] \\
BC1^{-}_{ns} &= \mu(k_n{}^2 - \beta_n{}^2)\left[De^{-ih\beta_n}\left(J_0(\varepsilon\beta_n) - iH_0(\varepsilon\beta_n)\right)\right] \\
BC2^{+}_{np} &= [\lambda(-k_n{}^2 - \eta_n{}^2) + 2\mu(-\eta_n{}^2)]\left[De^{ih\eta_n}\left(J_0(\varepsilon\eta_n) + iH_0(\varepsilon\eta_n)\right)\right] \\
BC2^{-}_{np} &= [\lambda(-k_n{}^2 - \eta_n{}^2) + 2\mu(-\eta_n{}^2)]\left[De^{-ih\eta_n}\left(J_0(\varepsilon\eta_n) - iH_0(\varepsilon\eta_n)\right)\right] \\
BC2^{+}_{ns} &= 2\mu(k_n\beta_n)\left[De^{ih\beta_n}\left(J_0(\varepsilon\beta_n) + iH_0(\varepsilon\beta_n)\right)\right] \\
BC2^{-}_{ns} &= -2\mu(k_n\beta_n)\left[De^{-ih\beta_n}\left(J_0(\varepsilon\beta_n) - iH_0(\varepsilon\beta_n)\right)\right] \\
BC3^{+}_{np} &= 2\mu(k_n\eta_n)\left[De^{-ih\eta_n}\left(J_0(\varepsilon\mu_n) - iH_0(\varepsilon\eta_n)\right)\right] \\
BC3^{-}_{np} &= -2\mu(k_n\eta_n)\left[De^{ih\eta_n}\left(J_0(\varepsilon\mu_n) + iH_0(\varepsilon\eta_n)\right)\right] \\
BC3^{+}_{ns} &= -\mu(k_n{}^2 - \beta_n{}^2)\left[De^{-ih\beta_n}\left(J_0(\varepsilon\beta_n) - iH_0(\varepsilon\beta_n)\right)\right] \\
BC3^{-}_{ns} &= -\mu(k_n{}^2 - \beta_n{}^2)\left[De^{ih\beta_n}\left(J_0(\varepsilon\beta_n) + iH_0(\varepsilon\beta_n)\right)\right] \\
BC4^{+}_{np} &= [\lambda(k_n{}^2 + \eta_n{}^2) + 2\mu(\eta_n{}^2)]\left[De^{-ih\eta_n}\left(J_0(\varepsilon\eta_n) - iH_0(\varepsilon\eta_n)\right)\right] \\
BC4^{-}_{np} &= [\lambda(k_n{}^2 + \eta_n{}^2) + 2\mu(\eta_n{}^2)]\left[De^{ih\eta_n}\left(J_0(\varepsilon\eta_n) + iH_0(\varepsilon\eta_n)\right)\right] \\
BC4^{+}_{ns} &= -2\mu(k_n\beta_n)\left[De^{-ih\beta_n}\left(J_0(\varepsilon\beta_n) - iH_0(\varepsilon\beta_n)\right)\right] \\
BC4^{-}_{ns} &= 2\mu(k_n\beta_n)\left[De^{ih\beta_n}\left(J_0(\varepsilon\beta_n) + iH_0(\varepsilon\beta_n)\right)\right]
\end{aligned}
\tag{4}
$$

where, the Struve function $H_n(z)$ appears in the solution of the inhomogeneous Bessel equation which for integer *n* has the form

$$
z^2\frac{d^2y}{dz^2} + z\frac{dy}{dz} + (z^2 - n^2)y = \frac{2}{\pi}\frac{z^{n+1}}{(2n-1)!!} \tag{5}
$$

the general solution of this equation consists of a linear combination of the Bessel functions $J_n(z)$ and the Struve functions $H_n(z)$.

Although the plate boundaries considered here are not pure sinusoidal, the geometry shown in Fig. 9 is the closest geometry to our problem for which theoretical solutions are available today. A comparison between Fig. 2c (true plate geometry) and Fig. 9 (plate geometry that has analytical solution) shows some common features between these two geometries, such as both plates have a periodicity with wavelength D, both have a maximum plate thickness H_1 and a minimum plate thickness H_2. Then the average plate thickness 2h is $(H_1+H_2)/2$ and the corrugation depth $2\varepsilon = (H_1 - H_2)/2$.

Analytically computed dispersion curves for the fundamental symmetric and anti-symmetric modes for the three plate geometries with 2h/D ratio equal to 1.078, 1.081, 0.905 and corresponding ε/D ratio equal to 0.049, 0.135 and 0.205, respectively are shown in Fig. 10. It should be noted here that although the geometry (Fig. 9) for the analytical solution is different from the specimen geometries (Fig. 2), two important parameters (2h/D and ε/D) are same for the analytical solution and the experimental investigation (listed in the right two columns of Table 1). Three plate geometries for the analytical solution are denoted as Specimens 1, 2 and 3, similar to the three plate specimens described in Table 1. Figure 10 shows the analytically computed Dispersion

curves for the three corrugated plates. In Fig. 10 the phase velocity is normalized with respect to the shear wave speed (3 km/s) in the plate material. The non-dimensional frequency (Ω) plotted along the horizontal axis is defined as

$$\Omega = \frac{\omega h}{c_S} \tag{6}$$

where, ω, h and c_S are identical to those in Eq. (1).

In the dispersion curves of Fig. 10 one can observe several discontinuities that are not observed in the dispersion curves for a smooth plate (see Fig. 8). The gaps in the dispersion curves are called the stop bands. It is interesting to note that as the corrugation depth increases the extent of the stop bands also increases. Experimentally it is also observed that the stop band zones increasing with the corrugation depth, see Figs. 6 and 7 – it gives a qualitative agreement between the experimental observations and theoretical predictions. For a quantitative comparison between the experimental and theoretical results, the non-dimensional frequency (Ω) and the normalized phase velocity c_L/c_S corresponding to the stop bands and pass bands shown in Table 2 are calculated and listed in Table 3.

As shown in Table 3, c_L/c_S is 0.993 and 1.175 for 30^o and 25^o angles of incidence, respectively. When the pass band and stop band frequencies are transformed from kHz (or MHz) to non-dimensional frequency (Ω) using Eq. (6) then the stop band 370-390 kHz for Specimen #1 is changed to 4.51-4.75 as shown in Table 3. When these stop bands (dashed lines) and pass bands (continuous lines) are plotted on the dispersion curves of Fig. 10 then sometimes good matching and some other times discrepancies between the theoretical curves and experimental stop and pass bands are observed. Since experiments are carried out for two different incident angles that correspond to two different c_L/c_S values (0.993 and 1.175) we get two horizontal lines corresponding to these two normalized velocities as shown in each plot of Fig. 10.

In Fig. 10a experimental stop bands (dashed lines) and pass bands (continuous lines) match very well with the theoretical dispersion curves. Note that the continuous lines either coincide or are located very close to the triangles (anti-symmetric modes) or circles (symmetric modes) while the dashed lines are seen in the regions where neither circles nor triangles are present. However, the matching between the experimental data (horizontal continuous lines at c_L/c_S = 0.993 and 1.175) and the theoretical values (triangles and circles) are not so good in Figs. 10b and 10c. Only matching that can be highlighted here is that in Fig. 10c in the non-dimensional frequency range 2.5 to 3.5 both theoretical and experimental values show stop bands.

From Fig. 10 it can be concluded that for small corrugation depth (when ε/D ratio is less than or equal to 0.05) the assumption of sinusoidal corrugation geometry is acceptable even when the actual geometry is not sinusoidal but periodic; however for large corrugation depth ($\varepsilon/D > 0.1$) the sinusoidal corrugation assumption does not work very well when the actual corrugation geometry is not sinusoidal.

Table 3: Non-dimensional frequencies (Ω) for stop and pass bands for 2 striking angles and 3 corrugated plate specimens whose dimensions are given in Table 1.

Striking Angle (θ)	**30°**	**30°**	**25°**	**25°**
$\frac{c_L}{c_S} = \frac{(1.49/\sin\theta)}{3}$	0.993	0.993	1.175	1.175
Specimen #1	**Stop Band frequency (MHz)**	**Pass Band frequency (MHz)**	**Stop Band frequency (MHz)**	**Pass Band frequency (MHz)**
Frequency (f) Range (in MHz)	0.370-0.390 0.470-0.490	0.300-0.370 0.390-0.470 0.490-0.650	0.300-0.350 0.375-0.410 0.465-0.510 0.580-0.610	0.350-0.375 0.410-0.465 0.510-0.580
Non-dimensional Frequency (Ω) $\left(\Omega = \frac{2\pi fh}{c_S} = \frac{11.63\pi f}{3} = 12.18\, f\right)$	4.51-4.75 5.72-5.97	3.65-4.51 4.75-5.72 5.97-7.92	3.65-4.26 4.57-4.99 5.66-6.21 7.06-7.43	4.26-4.57 4.99-5.66 6.21-7.06
Specimen #2	**Stop Band frequency (MHz)**	**Pass Band frequency (MHz)**	**Stop Band frequency (MHz)**	**Pass Band frequency (MHz)**
Frequency (f) Range (in MHz)	0.300-0.380 0.620-0.645	0.380-0.620 0.645-0.680	0.440-0.460 0.600-0.640	0.340-0.440 0.460-0.580
Non-dimensional Frequency (Ω) $\left(\Omega = \frac{2\pi fh}{c_S} = \frac{10.16\pi f}{3} = 10.64\, f\right)$	3.19-4.04 6.56-6.86	4.04-6.56 6.86-7.24	4.68-4.89 6.38-6.81	3.61-4.68 4.89-6.17
Specimen #3	**Stop Band frequency (MHz)**	**Pass Band frequency (MHz)**	**Stop Band frequency (MHz)**	**Pass Band frequency (MHz)**
Frequency (f) Range (in MHz)	0.300-0.450 0.580-0.600	0.450-0.580	0.300-0.390 0.470-0.530 0.590-0.650	0.390-0.470 0.530-0.590
Non-dimensional Stop Band Frequency (Ω) $\left(\Omega = \frac{2\pi fh}{c_S} = \frac{8.74\pi f}{3} = 9.15\, f\right)$	2.75-4.12 5.35-5.49	4.12-5.31	2.75-3.57 4.35-4.85 5.40-5.95	3.57-4.30 4.85-5.40

Conclusion:

The elastic wave propagation in homogeneous plates with periodic corrugated boundaries is experimentally investigated in this paper. Guided waves in three plates with three different degrees of corrugation are studied. Different stop bands and pass bands are observed for the three plates. The extent of stop bands is found to increase with the depth of corrugation. Experimental data generated by non-sinusoidal corrugated plates are compared with the theoretical predictions for sinusoidal corrugated plates. For small corrugation depth the theoretical and experimental data match reasonably well. However, for large corrugation depth the matching is not so good indicating that for large degree of corrugation the exact geometry of the plate boundary needs to be incorporated in the model. Only two parameters - the wavelength of periodicity and the depth of corrugation - are enough for correctly predicting the pass band and stop band regions in plates with small degree of corrugation but these two parameters are not enough for modeling wave propagation in plates with large degree of corrugation.

Acknowledgement:

This research was partially supported from a research grant from the Air Force Research Laboratory, AFRL/MLLP through CNDE (Center for Nondestructive Evaluation) of the Iowa State University and a grant from the National Science Foundation under the contract number CMS-9901221. Authors would also like to acknowledge the technical help of Mr. R. Reibel of UDRI/MLLP while carrying out the experiments.

References:

Banerjee, S., Kundu, T., (**2004**). "Analysis of wave propagation in symmetrically periodic sinusoidal wave-guide", *Health Monitoring and Smart Nondestructive Evaluation of Structural and Biological Systems*, Ed. T. Kundu, SPIE's 9th Annual International Symposium on NDE for Health Monitoring and Diagnostics, March 15-17, 2004, San Diego, California, Vol. **5394**, pp.89-98

Banerjee, S., Kundu, T., (**2006**), "Symmetric and Anti-symmetric Rayleigh-Lamb modes in Sinusoidally Corrugated Waveguides: An Analytical Approach", International Journal of Solids and Structures, in review.

Boström, A., (**1983**). "Passbands and Stopbands for an Electromagnetic waveguide with a periodically varying cross section". IEEE Transactions on Microwave Theory and Techniques, Vol. **31**, pp.752-756

Boström, A., (**1989**). "Propagating, damped, and leaky surface waves on the corrugated traction-free boundary of an elastic half-space". J. Acoust. Soc. Am., Vol. **85**, pp.1549-1555

Brillouin, L., (**1946**), *Wave Propagation in Periodic Structures*, Pub. Dover, New York.

Declercq, N. F., Degrieck, J., Briers, R., Leroy, O., (**2005**). "Diffraction of homogeneous and inhomogeneous plane waves on a doubly corrugated liquid/solid interface". Ultrasonics, Vol. **43** (8), pp.605-618

El-Bahrawy, A., (**1994a**). "Stopbands and Passbands for symmeetric Rayleigh-Lamb modes in a plate with corrugated surfaces". J. Sound and Vibration, Vol. **170**(2), pp.145-160.

El-Bahrawy, A., (**1994b**). "Point force excitation of surface waves along the doubly corrugated traction-free boundary of an elastic half-space". Comm. Div. Mech. **2**.

Fokkemma, J.H., (**1980**). "Reflection and transmission of elastic waves by the spatially periodic interface between two solids (Theory of integral-equation method)", Wave Motion, Vol. **2**, pp.375-393

Glass, N.E., Maradudin, A.A., (**1983**). "Leaky surface-elastic waves on both flat and strongly corrugated surfaces for isotropic, nondissipative media". J. Appl. Phys. Vol. **54**, pp.796-805

Kundu, T., **(2004)**. Chapter 1: Mechanics of Elastic Waves and Ultrasonic NDE, pp. 1-142, in *Ultrasonic Nondestructive Evaluation: Engineering and Biological Material Characterization*, Ed. T. Kundu, Pub. CRC Press.

Mead, D. J., (**1970**), "Free Wave Propagation in Periodically Supported, Infinite Beams", Journal of Sound and Vibration, Vol. **11**(2), pp. 181-197.

Mead, D. J., (**1975**), "Wave Propagation and Normal Modes in Periodic Systems: 1. Mono-Coupled Systems", Journal of Sound and Vibration, Vol. **40**(1), pp. 1-18.

Mead, D. J., (**1976**), "Loss Factors and Resonant Frequencies of Periodic Damped Sandwiched Plates", ASME Journal of Engineering for Industry, Vol. **98**, pp. 75-80.

Mead, D. J., (**1986**), "A New Method of Analyzing Wave Propagation in Periodic Structures: Applications to Periodic Timoshenko Beams and Stiffened Plates", Journal of Sound and Vibration, Vol. **104**(1), pp. 9-27.

Mead, D. J., Bardell, N. S., (**1987**), "Free Vibration of Thin Cylindrical Shell with Periodic Circumferential Stiffeners", Journal of Sound and Vibration, Vol. **115**(3), pp. 499-521.

Mead, D. J., Markus, S., (**1983**), "Coupled Flexural-Longitudinal Wave Motion in a Periodic Beam", Journal of Sound and Vibration, Vol. **90**(1), pp. 1-24.

Mead, D. J., Yaman, Y., (**1991**), "The Harmonic Response of Rectangular Sandwich Plates with Multiple Stiffening: A Flexural Wave Analysis", Journal of Sound and Vibration, Vol. **145**(3), pp. 409-428.

Mester, S. S., Benaroya, H., (**1995**), "Periodic and Near-Periodic Structures", Journal of Shock and Vibration, Vol.**2**(1), pp. 69-95

Nayfeh, A.H., Kandil, O.A., (**1978**). "Propagation waves in cylindrical hard-walled ducts with generally weak undulations". AIAA Journal, Vol. **16**, pp.1041-1045

Orris, R. M., Petyt, M., (**1974**), "A Finite Element Study of Harmonic Wave Propagation in Periodic Structures", Journal of Sound and Vibration, Vol. **33**(2), pp. 223-236

Russene, M., Baz, A., (**2000**), "Control of Wave Propagation in Periodic Composite Rods using Shape Memory Inserts", Journal of Vibration and Acoustics, Vol. **122**, pp. 151-159

Standström, S.E., (**1986**). "Stop bands in a corrugated parallel plate waveguide". J. Acoust. Soc. Am. Vol. **79**, pp.1293-1298

Vasseur, J. O., Deymier, P. A., Frantziskonis, G., Hong, G., Djafari-Rouhani, B., Dobrzynski, L., (**1998**), "Experimental Evidence for the Existence of Absolute

Acoustic Band Gaps in Two-Dimensional Periodic Composite Media", Journal of Physics: Condense Matter, Vol. **10**, pp. 6051-6064

Figure Caption:

Figure 1: (a) Two identical transducers placed face to face – one working as a transmitter and the second one as the receiver; (b) Received signal amplitude variation with frequency for the transmitter-receiver arrangement shown in Fig. 1(a).

Figure 2: Corrugated plate – (a) top view, (b) side view, (c) side view showing different dimensions.

Figure 3: Schematic of the transmitter (T), receiver (R) and the plate specimen arrangement. The direct reflected beam is shown by dashed lines. The receiver is placed beyond the direct reflection zone to detect the leaky guided waves.

Figure 4: Received signal voltage amplitude versus signal frequency curve or V(f) curve for a smooth plate specimen when the receiver is placed in the direct reflection zone marked by dashed lines in Fig. 3. Note the similarities between Figs. 1b and 4. [For this figure $\theta = 25^o$, h = 3 inch (76.2 mm) and d = 2.8 inch (71.1 mm), signal attenuation is 37 dB. Similar plot is obtained for h = 2.5 inch (63.5 mm) and d = 2.3 inch (58.4 mm)].

Figure 5: V(f) curve for a smooth plate specimen when the receiver is placed beyond the direct reflection zone as shown in Fig. 3. Note the changes in the V(f) curves of Figs. 4 and 5 in spite of the plate specimens for both figures being the same; the only difference is the horizontal distance (d) between the two transducers. For Fig. 5 the distance d is greater. [For this figure $\theta = 25^o$, h = 2.5 inch (63.5 mm) and d = 4.25 inch (108 mm), signal attenuation is 28 dB].

Figure 6: V(f) curves for three corrugated plate specimens when the transducer inclination angle is $\theta = 25^o$ and the receiver is placed beyond the direct reflection zone as shown in Fig. 3.
(a) V(f) curve for Specimen #1 (low corrugation, see Table 1) when h = 3 inch (76.2 mm) and d = 7 inch (177.8 mm), signal attenuation is 16 dB.
(b) V(f) curve for Specimen #2 (medium corrugation, see Table 1) when h = 3 inch (76.2 mm) and d = 7 inch (177.8 mm), signal attenuation is 14 dB.
(c) V(f) curve for Specimen #3 (large corrugation, see Table 1) when h = 3 inch (76.2 mm) and d = 7 inch (177.8 mm), signal attenuation is 18 dB.

Figure 7: V(f) curves for three corrugated plate specimens when the transducer inclination angle $\theta = 30^o$ and the receiver is placed beyond the direct reflection zone as shown in Fig. 3.

(a) V(f) curve for Specimen #1 (low corrugation, see Table 1) when h = 2.25 inch (57.2 mm) and d = 7.5 inch (190.5 mm), signal attenuation is 14 dB.
(b) V(f) curve for Specimen #2 (medium corrugation, see Table 1) when h = 2.25 inch (57.2 mm) and d = 7.5 inch (190.5 mm), signal attenuation is 10 dB.
(c) V(f) curve for Specimen #3 (large corrugation, see Table 1) when h = 2.25 inch (57.2 mm) and d = 7.5 inch (190.5 mm), signal attenuation is 15 dB.

Figure 8: Dispersion curves of 0.5 inch (12.7 mm) thick aluminum plate (c_P = 6.2 km/s, c_S = 3 km/s, ρ = 2.7 gm/cc). Two black circles are the experimental data points corresponding to the two peaks at 430 kHz and 645 kHz in the V(f) curve of Fig. 5, corresponding phase velocity V_{ph} = 3.526 km/s for 25^o angle of incidence is obtained from Snell's law (Eq. 2). Anti-symmetric and symmetric modes of order m are denoted by A_m and S_m, respectively.

Figure 9: Corrugated plate geometry with sinusoidal boundaries considered for the theoretical analysis. D = corrugation period, ε =corrugation depth, $2h$ = average plate thickness.

Figure 10: Symmetric (circles) and anti-symmetric (triangles) modes computed theoretically from Eq. for three plate specimens (10a – small corrugation, Specimen #1; 10b – medium corrugation, Specimen #2; 10c – large corrugation, Specimen #3). See Table 1 for specimen dimensions. Experimentally obtained stop bands (dashed lines) and pass bands (continuous lines) for two normalized phase velocities (0.993 corresponds to 30^o striking angle and 1.175 for 25^o striking angle) are shown in each plot. In Fig. 10a pass bands match very well with the theoretical values. However, the matching between the theoretical and experimental values is not so good in Figs. 10b and 10c.

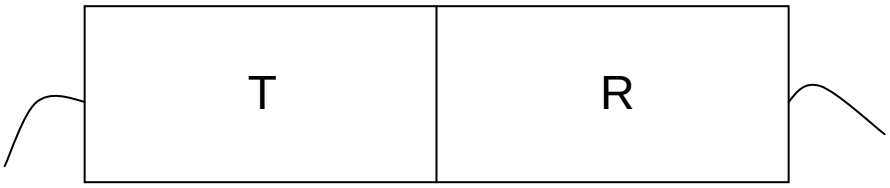

(a)

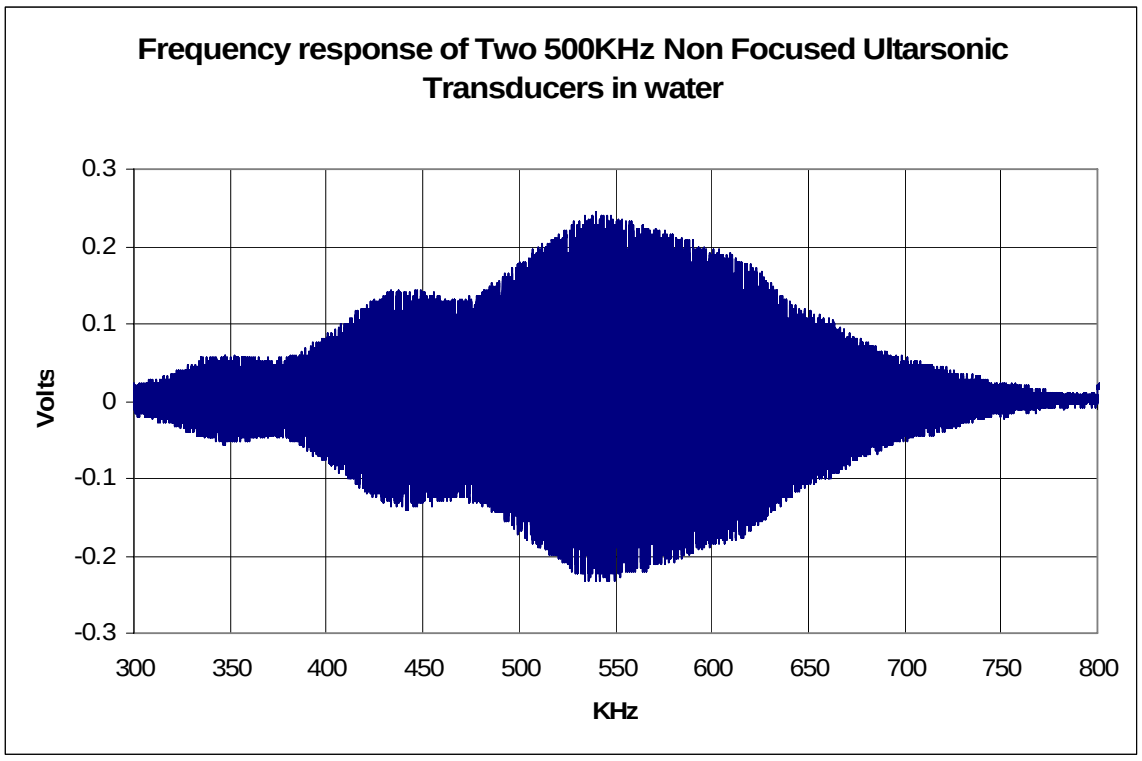

(b)

Figure 1: (a) Two identical transducers placed face to face – one working as a transmitter and the second one as the receiver; (b) Received signal amplitude variation with frequency for the transmitter-receiver arrangement shown in Fig. 1(a).

(a)

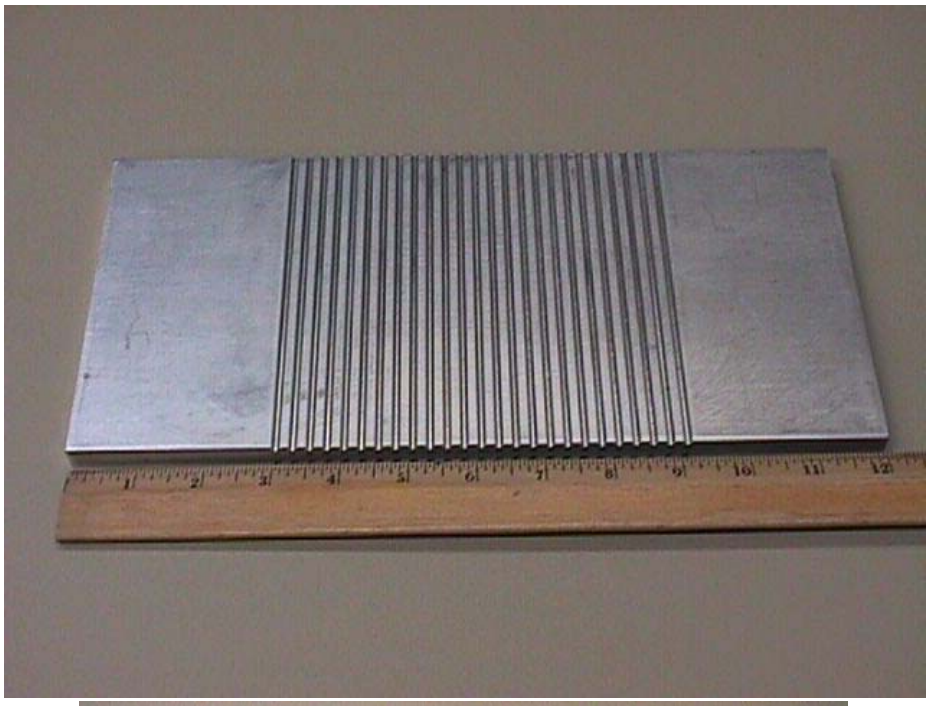

(b)

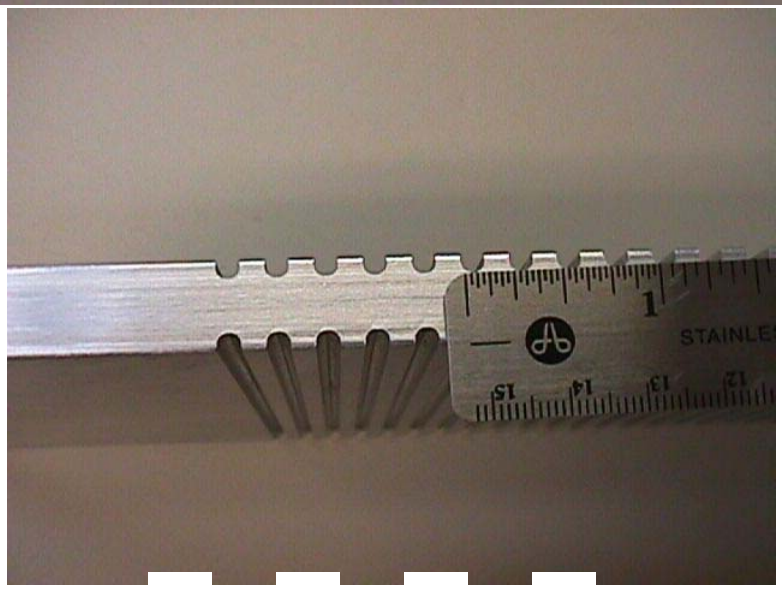

(c)

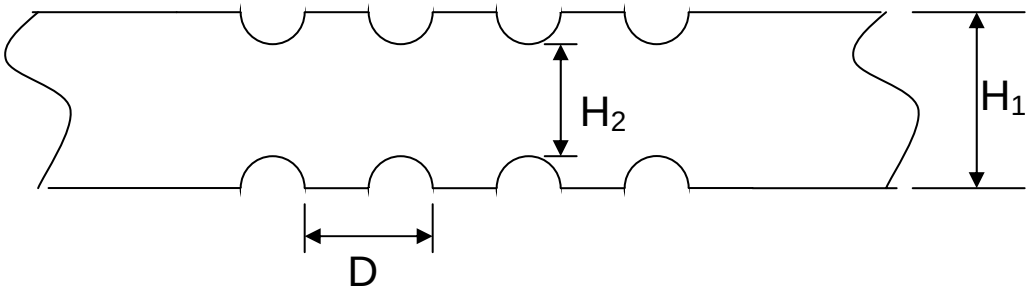

Figure 2: Corrugated plate – (a) top view, (b) side view, (c) side view showing different dimensions.

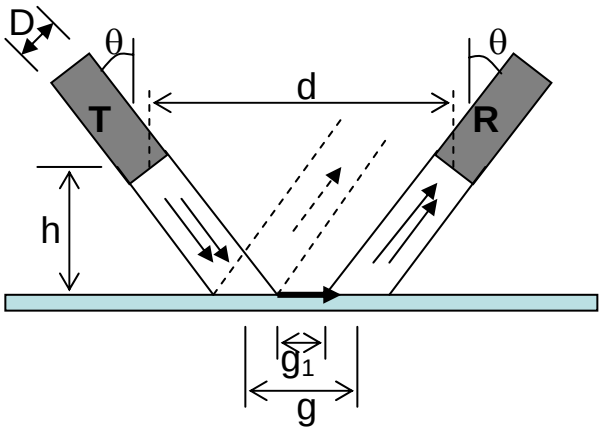

Figure 3: Schematic of the transmitter (T), receiver (R) and the plate specimen arrangement. The direct reflected beam is shown by dashed lines. The receiver is placed beyond the direct reflection zone to detect the leaky guided waves

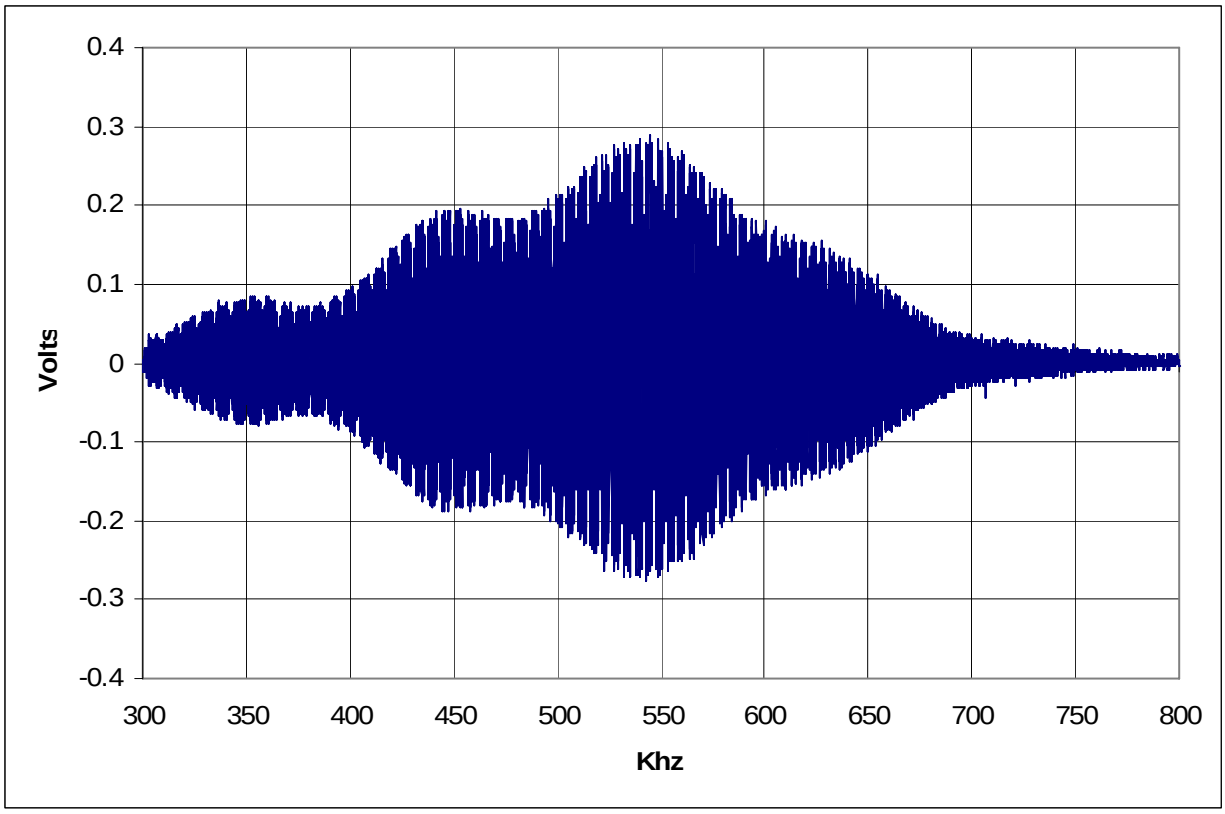

Figure 4: Received signal voltage amplitude versus signal frequency curve or V(f) curve for a smooth plate specimen when the receiver is placed in the direct reflection zone marked by dashed lines in Fig. 3. Note the similarities between Figs. 1b and 4. [For this figure $\theta = 25^{o}$, h = 3 inch (76.2 mm) and d = 2.8 inch (71.1 mm), signal attenuation is 37 dB. Similar plot is obtained for h = 2.5 inch (63.5 mm) and d = 2.3 inch (58.4 mm)]

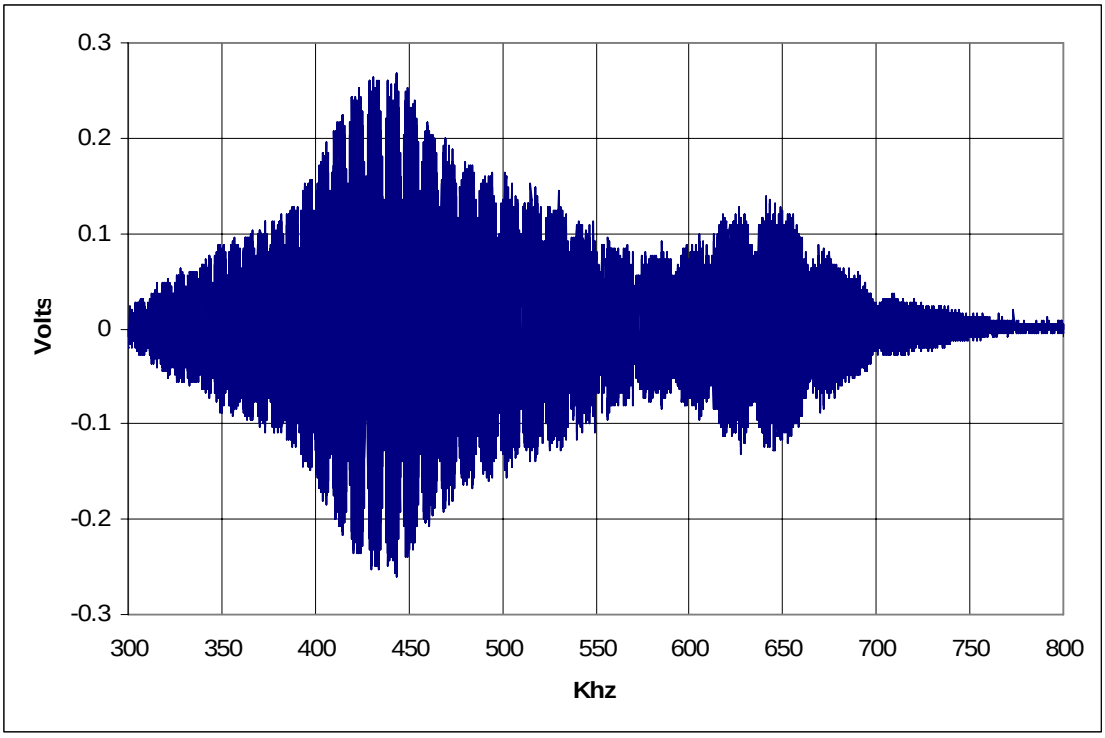

Figure 5: V(f) curve for a smooth plate specimen when the receiver is placed beyond the direct reflection zone as shown in Fig. 3. Note the changes in the V(f) curves of Figs. 4 and 5 in spite of the plate specimens for both figures being the same; the only difference is the horizontal distance (d) between the two transducers. For Fig. 5 the distance d is greater. [For this figure $\theta = 25^{o}$, h = 2.5 inch (63.5 mm) and d = 4.25 inch (108 mm), signal attenuation is 28 dB].

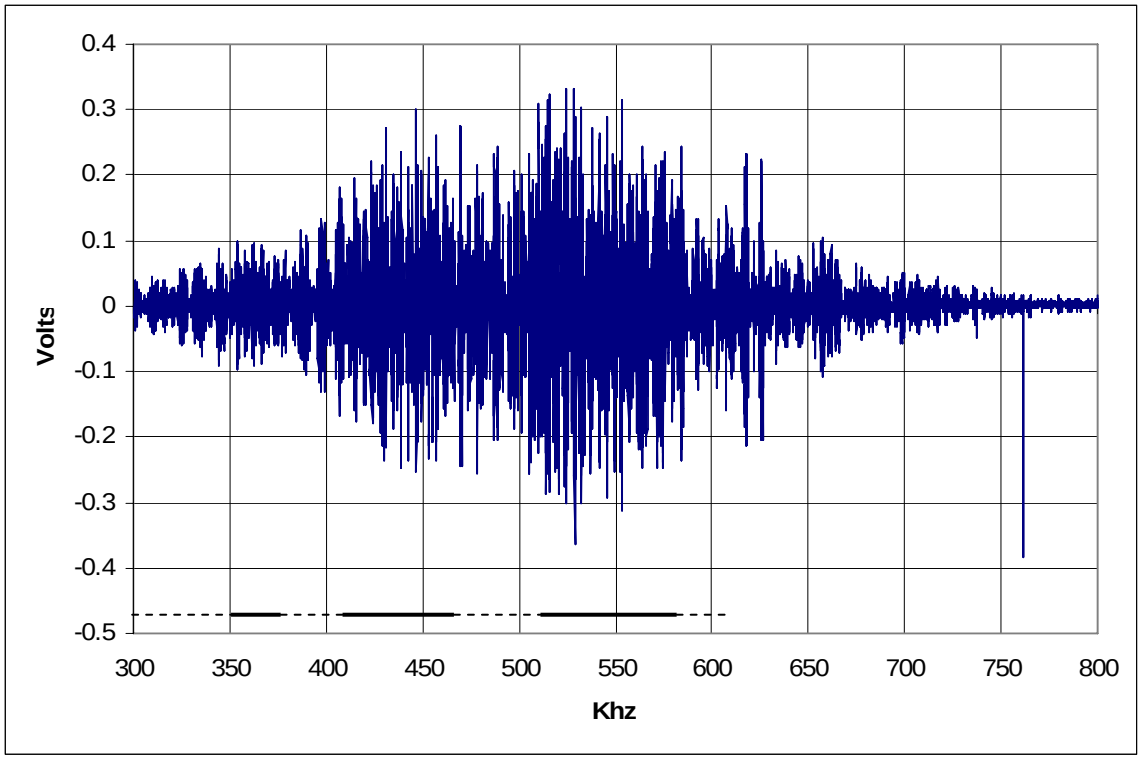
0.4
0.3
0.2
0.1
0
-0.1
-0.2
-0.3
-0.4
-0.5
Volts
300
350
400
450
500
550
600
650
700
750
800
Khz

Fig. 6a

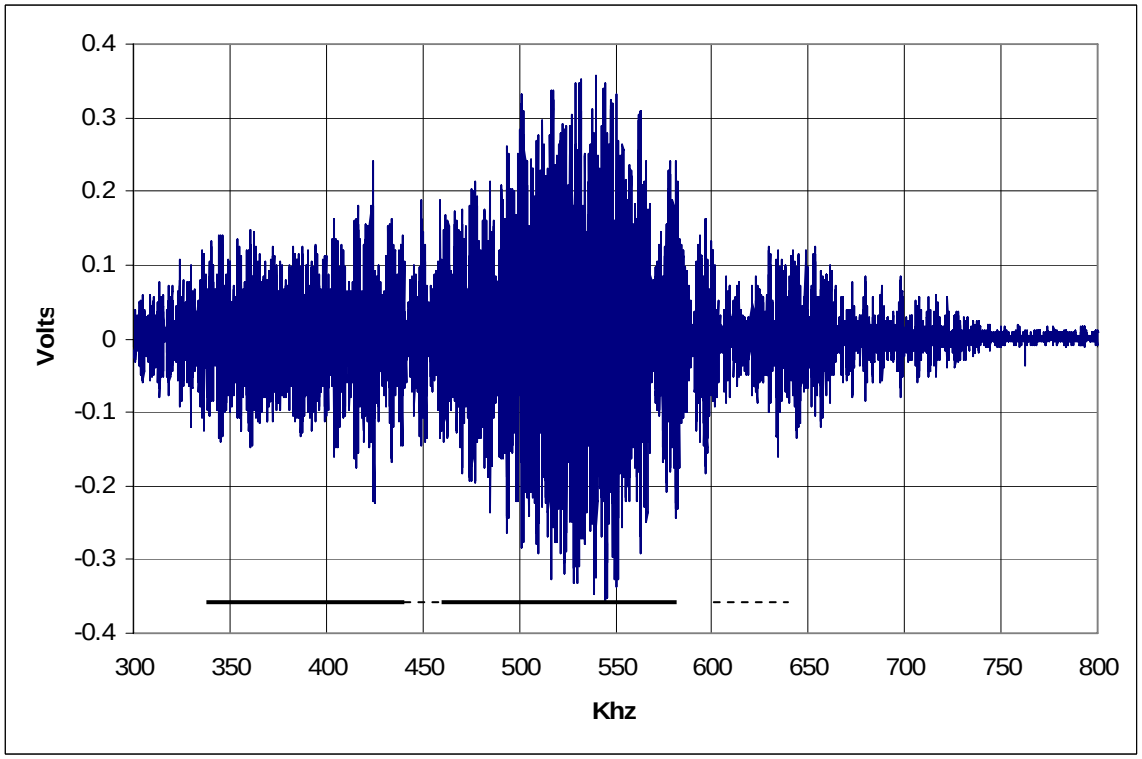
0.4
0.3
0.2
0.1
0
-0.1
-0.2
-0.3
-0.4
Volts
300
350
400
450
500
550
600
650
700
750
800
Khz

Fig. 6b

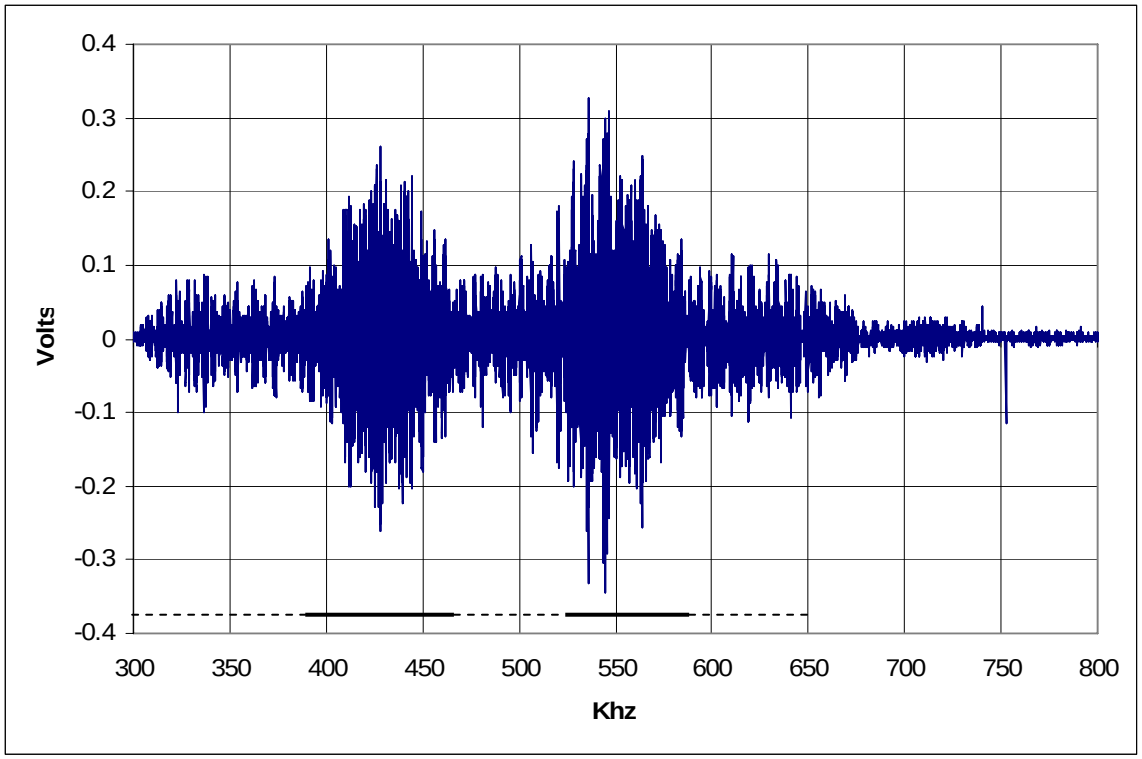

Fig. 6c

Figure 6: V(f) curves for three corrugated plate specimens when the transducer inclination angle is $\theta = 25^{o}$ and the receiver is placed beyond the direct reflection zone as shown in Fig. 3.
(a) V(f) curve for Specimen #1 (low corrugation, see Table 1) when h = 3 inch (76.2 mm) and d = 7 inch (177.8 mm), signal attenuation is 16 dB.
(b) V(f) curve for Specimen #2 (medium corrugation, see Table 1) when h = 3 inch (76.2 mm) and d = 7 inch (177.8 mm), signal attenuation is 14 dB.
(c) V(f) curve for Specimen #3 (large corrugation, see Table 1) when h = 3 inch (76.2 mm) and d = 7 inch (177.8 mm), signal attenuation is 18 dB.

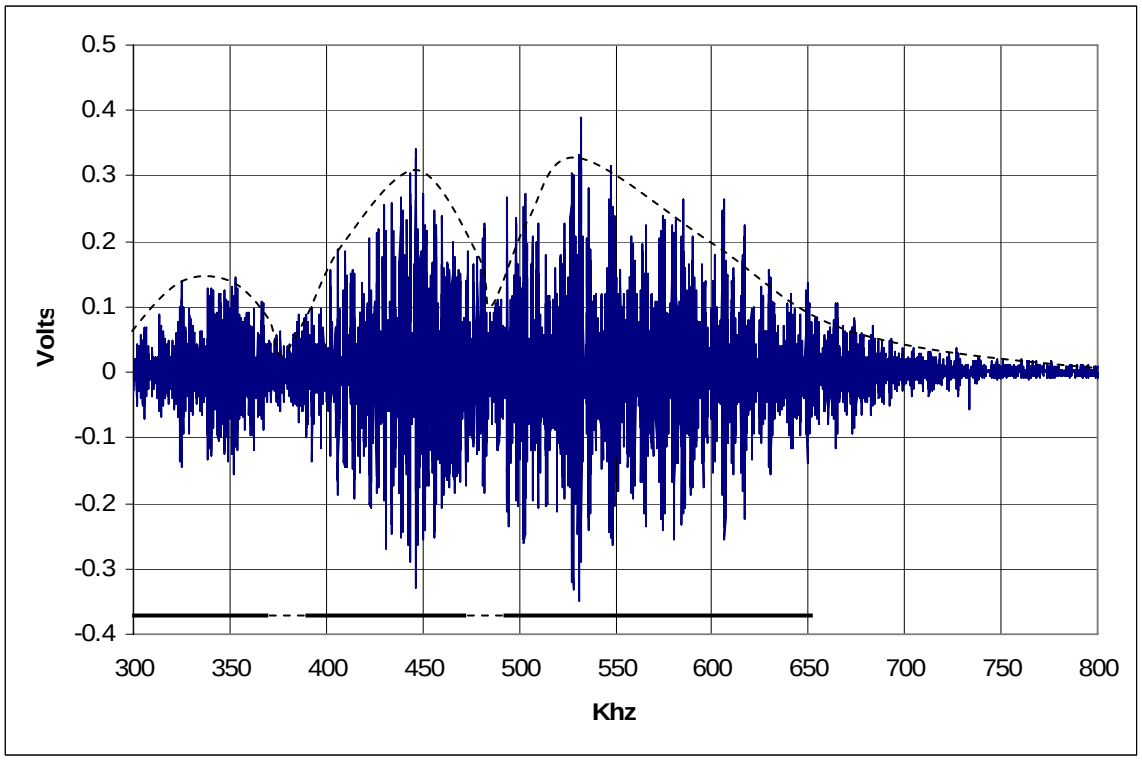
0.5
0.4
0.3
0.2
0.1
0
-0.1
-0.2
-0.3
-0.4
Volts
300
350
400
450
500
550
600
650
700
750
800
Khz

Fig. 7a

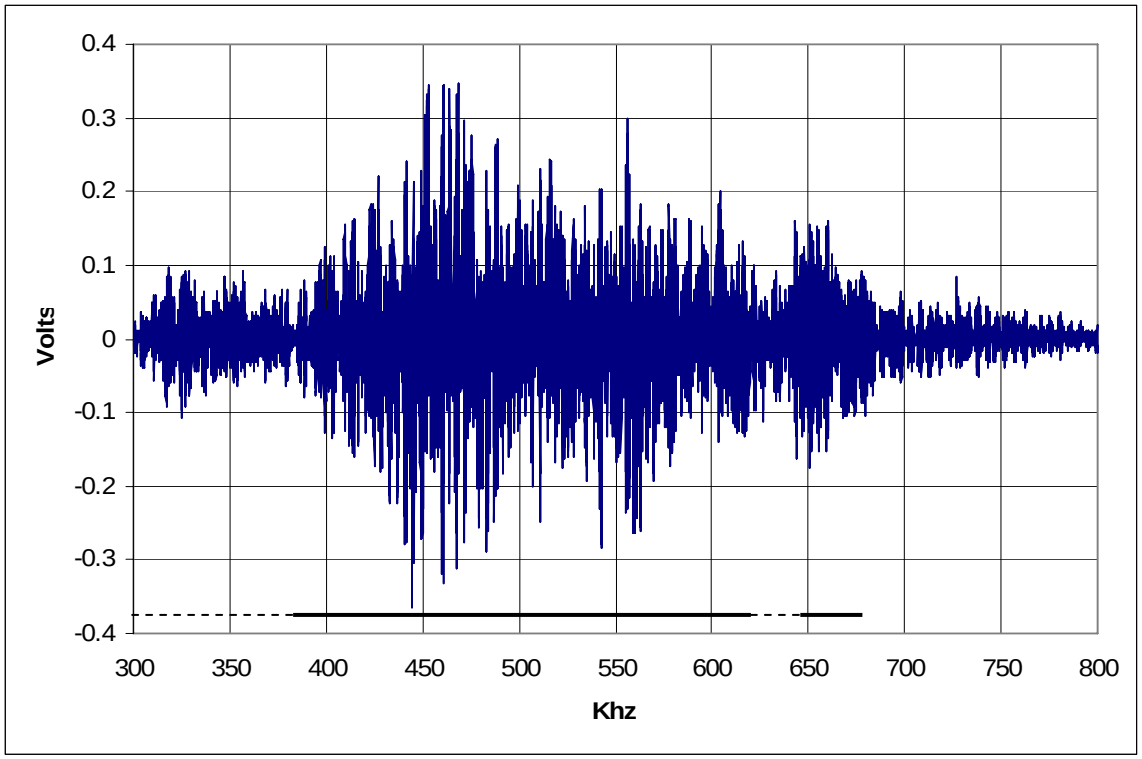
0.4
0.3
0.2
0.1
0
-0.1
-0.2
-0.3
-0.4
Volts
300
350
400
450
500
550
600
650
700
750
800
Khz

Fig. 7b

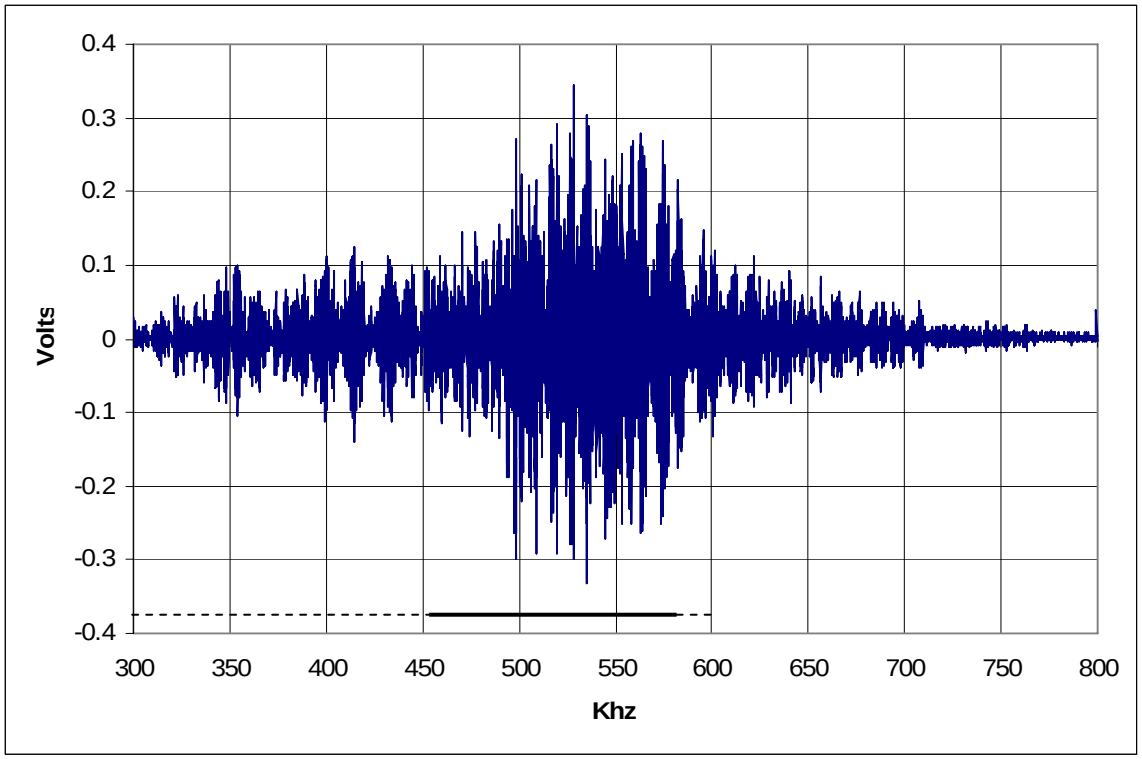

Fig. 7c

Figure 7: V(f) curves for three corrugated plate specimens when the transducer inclination angle $\theta = 30^{o}$ and the receiver is placed beyond the direct reflection zone as shown in Fig. 3.
(a) V(f) curve for Specimen #1 (low corrugation, see Table 1) when h = 2.25 inch (57.2 mm) and d = 7.5 inch (190.5 mm), signal attenuation is 14 dB.
(b) V(f) curve for Specimen #2 (medium corrugation, see Table 1) when h = 2.25 inch (57.2 mm) and d = 7.5 inch (190.5 mm), signal attenuation is 10 dB.
(c) V(f) curve for Specimen #3 (large corrugation, see Table 1) when h = 2.25 inch (57.2 mm) and d = 7.5 inch (190.5 mm), signal attenuation is 15 dB.

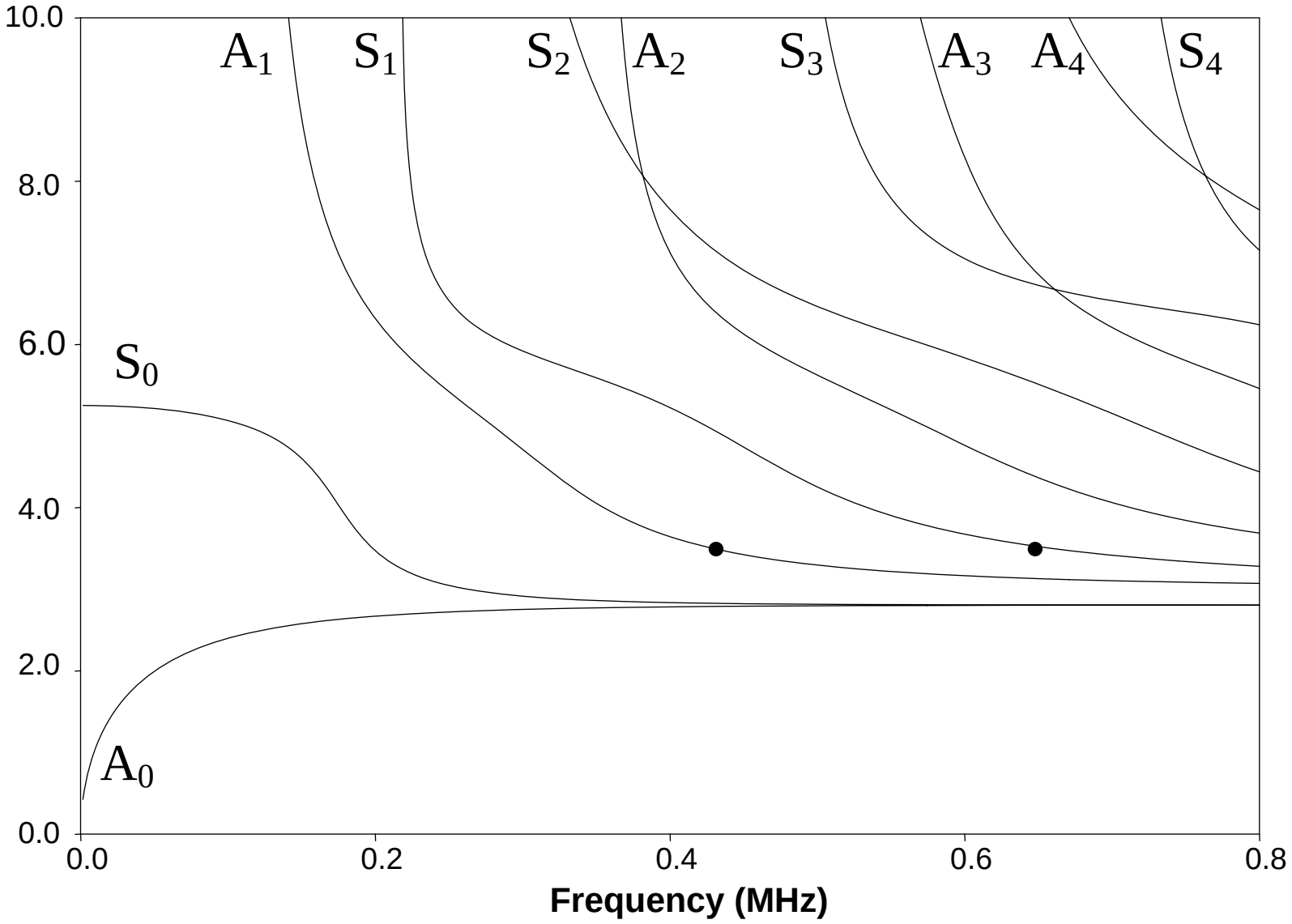

Figure 8: Dispersion curves of 0.5 inch (12.7 mm) thick aluminum plate (c_P = 6.2 km/s, c_S = 3 km/s, ρ = 2.7 gm/cc). Two black circles are the experimental data points corresponding to the two peaks at 430 kHz and 645 kHz in the V(f) curve of Fig. 5, corresponding phase velocity V_{ph} = 3.526 km/s for 25^o angle of incidence is obtained from Snell's law (Eq. 2). Anti-symmetric and symmetric modes of order m are denoted by A_m and S_m, respectively.

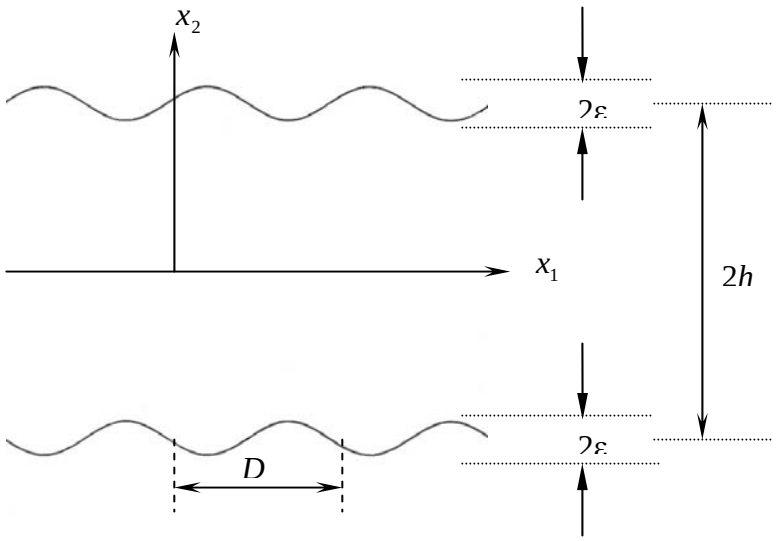

Figure 9: Corrugated plate geometry with sinusoidal boundaries considered for the theoretical analysis. D = corrugation period, ε =corrugation depth, $2h$ = average plate thickness.

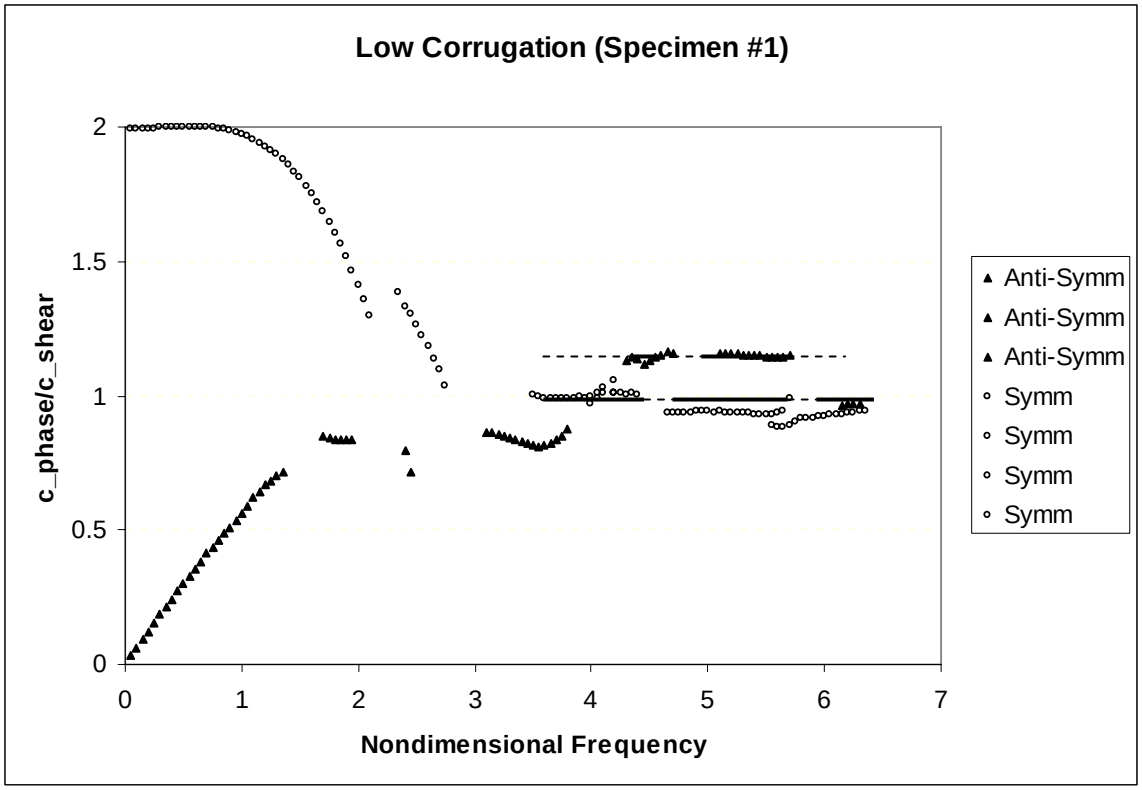

Fig. 10a

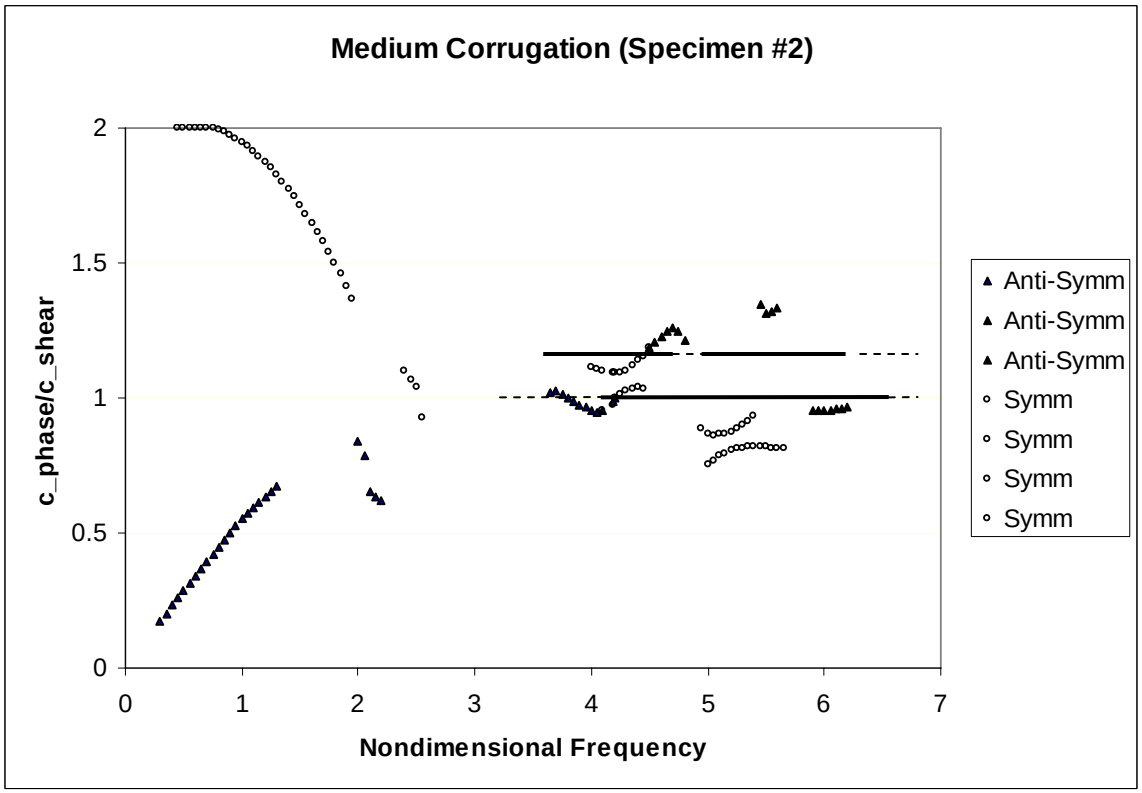

Fig.10b

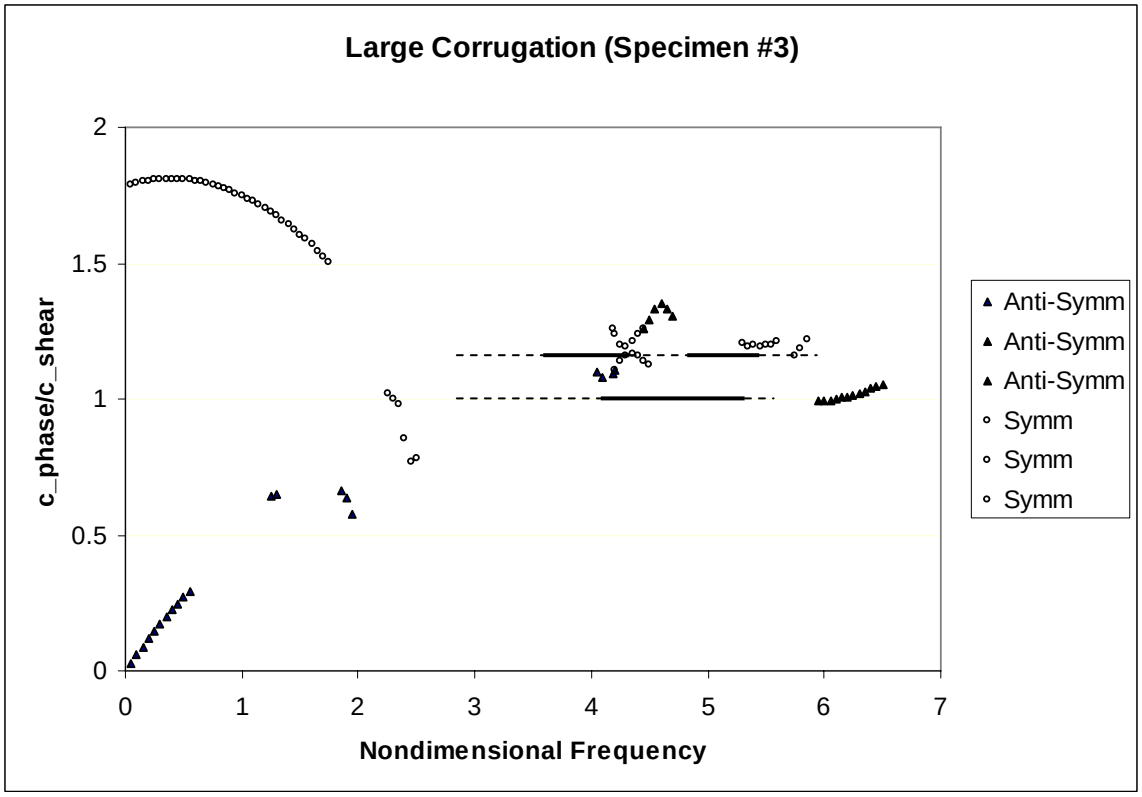

Fig. 10c

Figure 10: Symmetric (circles) and anti-symmetric (triangles) modes computed theoretically from Eq. for three plate specimens (10a – small corrugation, Specimen #1; 10b – medium corrugation, Specimen #2; 10c – large corrugation, Specimen #3). See Table 1 for specimen dimensions. Experimentally obtained stop bands (dashed lines) and pass bands (continuous lines) for two normalized phase velocities (0.993 corresponds to 30^o striking angle and 1.175 for 25^o striking angle) are shown in each plot. In Fig. 10a pass bands match very well with the theoretical values. However, the matching between the theoretical and experimental values is not so good in Figs. 10b and 10c.